Mechanisms of size segregation in granular flows with different ambient fluids

Kahlil Fredrick Cui[1,2], *Gordon G.D.* Zhou[1,2,3*], and *Lu* Jing[4]

[1]Key Laboratory of Mountain Hazards and Earth Surface Process / Institute of Mountain Hazards and Environment, Chinese Academy of Sciences, Chengdu 610000, China
[2]University of Chinese Academy of Sciences, Beijing 100000, China
[3]China-Pakistan Joint Research Center on Earth Sciences, CAS-HEC
[4]Department of Chemical and Biological Engineering, Northwestern University, Evanston, IL 60208, USA

Abstract. Particle size segregation is ubiquitous in granular systems with differently sized constituents but is found to diminish in the presence of viscous ambient fluids. We study this inhibiting effect through coupled fluid-particle numerical simulations. It is found that size segregation is indeed slower in the presence of fluid and this effect becomes more significant as fluid viscosity is increased. Direct calculation of segregation forcing terms reveal that the ambient fluids affect segregation in two major ways: buoyant forces reduce contact pressures, while viscous dissipation diminish particle-fluctuation driven kinetic pressures, both of which are necessary in driving large particles up. Surprisingly, the fluid drag in the normal direction is negligible regardless of the fluid viscosity and does not directly affect segregation.

1 Introduction

Granular flows consisting of differently sized particles have a tendency to segregate into homogeneous layers where large particles rise to the free-surface and small particles settle to the base. In the absence of a viscous interstitial fluid, small particles preferentially fall down into randomly generated voids, while the large particles are rolled upwards due to re-arrangement and persistent contacts of their surrounding particles [1–4]. Competing with upward and downward percolation is the tendency of particles to diffuse owing to random collisions and shearing of particles over each other [5].

Real-world granular flows, however, are either fluid saturated [6] or entirely submerged [7], in which cases solid-fluid interactions become significant and particle segregation may be effectively inhibited. Although a theoretical model has been proposed to capture this inhibitive effect [8], our understanding of its mechanical origins is still incomplete. Specifically, it is interesting to know how fluid forces such as fluid drag and buoyancy affect this process. Evaluation of these fluid effects will ultimately enable better prediction of grading patterns in granular-fluid mixtures.

This work aims to isolate and evaluate different effects of ambient fluids on particle size segregation. To this end, three-dimensional fluid-particle numerical simulations of simplified, bidisperse immersed granular flows are conducted using the coupled CFD-DEM. The process of segregation in different ambient fluids is analyzed according to segregation forcing terms derived from mixture theory [8] and stress partitioning.

2 Segregation forcing terms and stress partitioning

The three-phase mixture theory of segregation [8] deals with the evolution of partial variables defined per unit volume V_M. We consider a mixture of bidisperse particles, composed of large L and small S particles with a viscous interstitial fluid F, moving down an incline at a constant angle θ, in a coordinate system where the z-axis is pointing upward normal to the flow base, the x-axis along the direction of the flow, and the y-axis across the flow surface. For simplicity, we assume that the flow is incompressible and shallow in steady state. It is also assumed that segregation only occurs normal to the flow direction. Focusing on the *granular phase*, Ref. [8] shows that the governing momentum equation can be reduced to:

$$0 = -\frac{\partial \sigma_{zz,i}}{\partial z} - \Phi_i \rho_i g \cos\theta + \beta \qquad (1)$$

where an index $i = L, S$ is used to collectively represent large- and small-particle phases. Φ_i is the volume fraction of particle size phases, ρ_i is the material density, and g is the acceleration due to gravity. For simplicity, we consider the normal stress as the pressure $P = \sigma_{zz}$. The solid concentration ϕ_i is the ratio between Φ_i and the total granular volume fraction $\boldsymbol{\Phi} = \Phi_L + \Phi_S$.

Following Ref. [9], we decompose the pressure experienced by a particle phase into contact and kinetic components, i.e. $P_i = P_i^c + P_i^k$, representing the stresses which result from particle contacts and velocity

* Corresponding author: gordon@imde.ac.cn

A video is available at https://doi.org/10.48448/z95r-de64

© The Authors, published by EDP Sciences. This is an open access article distributed under the terms of the Creative Commons Attribution License 4.0 (http://creativecommons.org/licenses/by/4.0/).

fluctuations, respectively. The main idea behind segregation theory is that large (small) particles bear more (less) of the upward (downward) stress than they should according to their volume fraction. The fraction of pressure experienced by each phase is calculated as:

$$\psi_i^c = P_i^c/P^c \quad \text{and} \quad \psi_i^k = P_i^k/P^k \tag{2}$$

Pressure fractions are assumed to satisfy the functional forms:

$$\begin{aligned} \psi_{L,S}^c &= \phi_{L,S} \pm B^c \phi_S \phi_L \\ \psi_{L,S}^k &= \phi_{L,S} \pm B^k \phi_S \phi_L \end{aligned} \tag{3}$$

respectively, such that $\psi_L^{c,k} + \psi_S^{c,k} = 1$, and $\psi_i^{c,k} = 0$ for $\phi_i = 0$ [5]. The coefficients B^c and B^k are the magnitudes of the 'overstress' which lead the partial pressures away from the hydrostatic pressure and indicate the strength of the segregation driving force.

The third term on the right-hand side of Eq. (1) is the force exerted by one of the constituent phases on the others. The force exerted by one solid component on the other $\beta^{L\leftrightarrow S}$:

$$\beta^{L\leftrightarrow S} = -\Phi_i \rho_i c_{PD}(\boldsymbol{U_i} - \boldsymbol{U_G}) - \boldsymbol{\Phi} \rho_G c_D \nabla \phi_i \tag{4}$$

is a linear combination of the contributions from the relative velocity of the particle size specie $\boldsymbol{U_i}$ with the solid bulk $\boldsymbol{U_G}$, and the diffusive remixing [5]. The coefficients c_{PD} and c_D determine the strength of inter-phase drag and diffusion respectively.

Here we consider that the force exerted by the solid and fluid phases on each other can be expressed as:

$$\beta^{G\leftrightarrow F} = \left(\boldsymbol{F}_i^b + \boldsymbol{F}_i^d\right)/V_M. \tag{5}$$

$\boldsymbol{F}_i^b$ is the buoyant force which is calculated as:

$$\boldsymbol{F}_i^b = -\sum_j V_{ij} \nabla P_F \tag{6}$$

where V_{ij} is the volume of a particle j of phase i and ∇P_F is the fluid pressure gradient. $\boldsymbol{F}_i^d$ is the drag force which is calculated as:

$$\boldsymbol{F}_i^d = \sum_j \frac{1}{2} C_d \rho_F \frac{\pi D_{ij}^2}{4} \left(\boldsymbol{U}_F - \boldsymbol{U_{ij}}\right)^2 (1-\Phi_i)^{-\chi} \tag{7}$$

where D_{ij} and $\boldsymbol{U_{ij}}$ are the diameter and velocity a particle j of phase i. ρ_F, and $\boldsymbol{U}_F$, are the fluid density and flow velocity, respectively and $(1-\Phi_i)^{-\chi}$ is a porosity correction coefficient [10] which reflects the effect of granular concentration on the drag force. The drag force coefficient C_d used is that of Ref. [11]. Since the interaction terms are internal forces, they should cancel as Eq. 1 is summed over all phases, i.e. $\beta^{L-S} + \beta^{S-L} = 0$ and $\beta^{G-F} + \beta^{F-G} = 0$.

Combining Eqs. 2-7, into Eq. 1, we get:

$$0 = \Theta_i^{CS} + \Theta_i^{KS} + \Theta_i^W + \Theta_i^{PD} + \Theta_i^{FD} + \Theta_i^D \tag{8}$$

where:

$$\begin{aligned} \Theta_i^{CS} &= -\frac{\partial P_i^c}{\partial z} \\ \Theta_i^{KS} &= -\frac{\partial P_i^k}{\partial z} \\ \Theta_i^W &= -\Phi_i \rho_i g \cos\theta + \boldsymbol{F}_i^b/V_M \\ \Theta_i^{PD} &= -\Phi_i \rho_i c_{PD}(\boldsymbol{w_i} - \boldsymbol{w_G}) \\ \Theta_i^{FD} &= \boldsymbol{F}_i^d/V_M \\ \Theta_i^D &= -\rho_G c_D \frac{\partial \phi_i}{\partial z} \end{aligned} \tag{9}$$

Eq. 9 implies that the forces acting on a particle phase i as it segregates are due to the partial contact stress gradient Θ_i^{CS}, partial kinetic stress gradient Θ_i^{KS}, particle-particle drag Θ_i^{PD}, fluid drag Θ_i^{FD}, and diffusion Θ_i^D. The buoyant weight Θ_i^W takes into account the fluid buoyant effect.

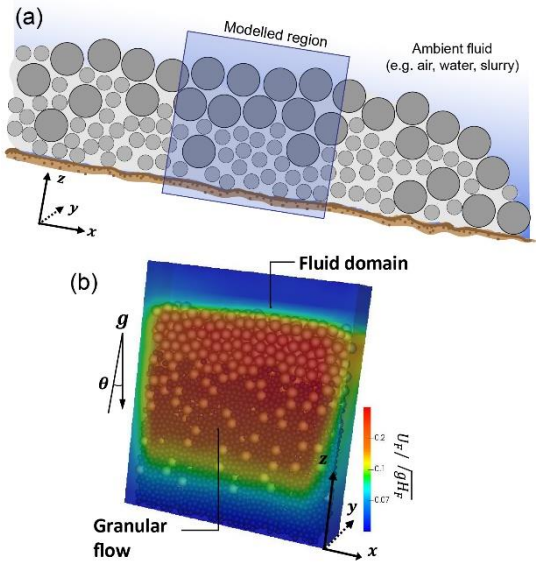

Fig. 1. (a) A schematic diagram of the modelled system and (b) illustration of an actual simulated case which is similar to the encased region in (a).

3 Set up

Three-dimensional, granular flows in ambient fluids are simulated using the coupled CFD-DEM – a numerical method that couples computational fluid dynamics (CFD) with the discrete element method (DEM) through a message passing algorithm that allows two open source solvers to communicate after a set number of time steps. The CFD-DEM is well-validated and has been widely used in modelling solid-particle interactions relevant to industrial and geophysical systems. A detailed description of this computational method can be found in Ref. [10].

Bidisperse granular flows are simulated as a mixture of small and large particles with diameters of $d_S = 0.005\,\text{m}$ and $d_L = 0.01\,\text{m}$ respectively. The floor is roughened by 'gluing' a random array of small particles. The mixture is initially normally graded. Periodic boundaries are set along the streamwise direction and flows are initiated from rest by tilting the xy plane to a constant angle of inclination. Particle contacts are simulated using a spring-dashpot contact model with Young's modulus 5×10^7 Pa, Poisson's ratio 0.35, coefficients of restitution 0.8 and friction 0.5.

The fluid domain is an incompressible Newtonian fluid, uniformly discretized in such a way that at least five large particles would fit [10]. The fluid is ambient – it only responds to the drag exerted by the particles and does not flow on its own under gravity. In this study, three types of ambient fluids are used – air ($\rho_F = 1.29\,\text{kg/m}^3, \eta_F = 1.85 \times 10^{-5}\,\text{kg/m}\cdot\text{s}$), water ($\rho_F = 1000\,\text{kg/m}^3, \eta_F = 1.\times 10^{-3}\,\text{kg/m}\cdot\text{s}$), and a viscous 'slurry' ($\rho_F = 1000\,\text{kg/m}^3, \eta_F = 0.5\,\text{kg/m}\cdot\text{s}$).

The schematic diagram of the system and the complete simulation set-up is shown in Fig. 1. The set-

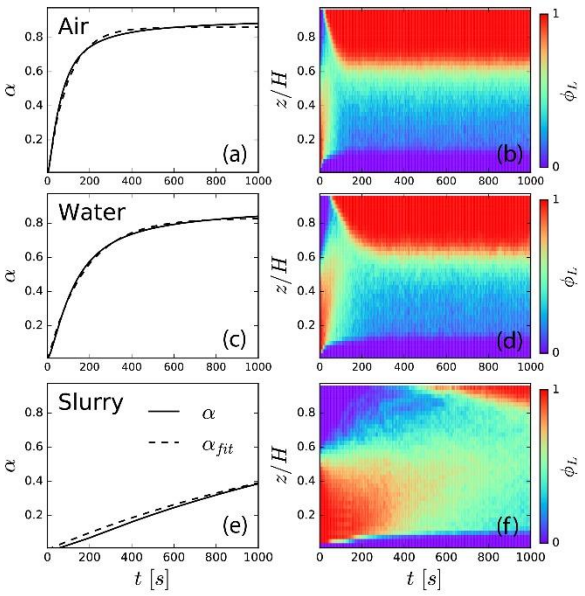

Fig. 2. The temporal evolution of the segregation degree α of a mixture flowing in (a) air, (c) water, and (d) viscous slurry and the corresponding spatial-temporal profile of the large particle concentration (b, d, f).

up is akin to section of an infinitely long submarine flow. The solid domain is positioned completely within the fluid domain and drags the fluid into motion.

4 Results

4.1 Process of segregation

Fig. 2 shows the progress of segregation measured by α which is calculated as:

$$\alpha(t) = 0.5\left(1 - \frac{C_{L,t} - C_{S,t}}{C_{L,0} - C_{S,0}}\right) \tag{10}$$

where $C_{L,t}$ and $C_{S,t}$ are the bulk centers of mass of the large and small particles at time t, respectively, while $C_{L,0}$ and $C_{S,0}$ are the initial bulk centers of mass. With this definition, $\alpha = 0$ is the initial state specific to our system and $\alpha = 1$ represents perfect inverse grading. At early times, α rapidly increases until it reaches a steady state. The time evolution of α follows an exponential trend which can be fit to:

$$\alpha_{fit}(t) = \alpha_f\left(1 - e^{-t/t_s}\right) \tag{11}$$

where α_f is the final degree of segregation and t_s is the dimensionless characteristic timescale associated with

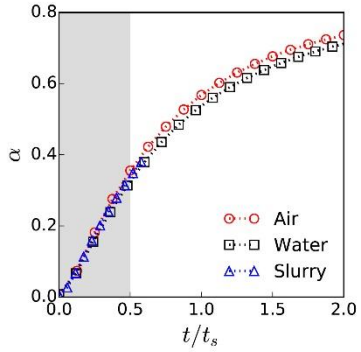

Fig. 3. The evolution of α in dimensionless time. Shaded region represents the span of time in which the segregation in different ambient fluids occur at the same pace.

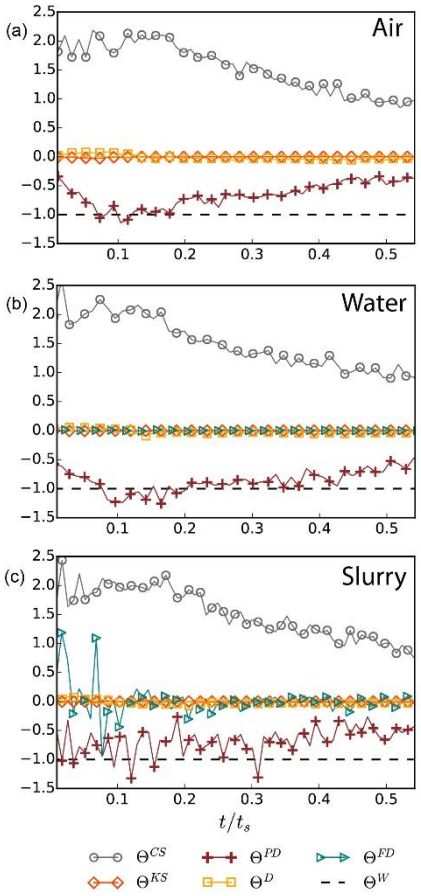

Fig. 4. The evolution of depth-averaged segregation forcing terms evaluated in Eq. 9 for different ambient fluids.

the segregation rate. Segregation in the presence of fluid is indeed slower and becomes more so in more viscous fluids. The process of segregation in slurry is still at its early-stages and has not reached steady-state even after 1000 seconds. Figs. 2b, d, f illustrate the spatial-temporal distribution of ϕ_L to show how well α defines the progress of segregation.

4.2 Segregation forcing terms

Fig. 3 shows that the rate of the segregation process in different fluids can be cast into a single timeframe using the dimensionless time t/t_s. Fig. 4 shows the depth-averaged 'forces' acting on the rising large particles in the normal direction for mixtures in different ambient fluids for $t = (0{\sim}0.5)t_s$ (shaded region in Fig. 3). In this way, the forces acting on the large particles can be compared directly during the time in which segregation in the three ambient fluids occur at the same pace. All force terms are normalized by Θ^W prior to depth averaging.

The difference between Θ^{CS} and Θ^W is mainly balanced by the particle-particle drag Θ^{PD} and only slightly by the diffusive force Θ^D, while the fluid-particle drag Θ^{FD} is practically negligible in both water and viscous slurry. Θ^{KS} is consistently small in all cases. Close evaluation of the fluid drag force shows that, since segregation proceeds slowly in the slurry the relative velocities between the large particles and the fluid along the normal direction are small resulting to minimal drag

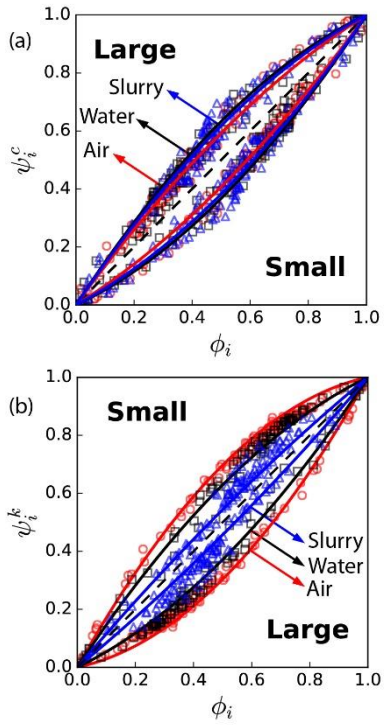

Fig. 5. (a) ψ_i^c and (b) ψ_i^k as a function of the volume concentration ϕ_i during rapid segregation in different ambient fluids.

force. Results in Fig. 4 suggest that segregation occurs when the partial normal stress gradient in the mixture overcomes the particles' buoyant weight, as is the premise of gravity-driven segregation theory [3]. However, this cannot account for the decrease in the segregation rate as the fluid becomes more viscous since the relative magnitude of Θ^{CS} with Θ^{W} remains constant across all fluids, i.e. although buoyant forces reduce particle contact forces, they proportionately decrease the particles' effective weight. To further investigate the effects of fluid viscosity on segregation, a more localized approach is adopted here to take the local concentration into account.

4.3 Analysis using stress partitioning

The contact stress fraction ψ_i^c in different ambient fluids are plotted as functions of ϕ_i in Fig. 5a. The ψ_L^c values are larger than ϕ_L, which means that large particles bear more of the contact pressure P^c than their volume fraction, causing them to rise. The opposite is true for small particles. The $\psi_i^c - \phi_i$ curves in air, water, and viscous slurry closely overlap which is consistent with the invariance of Θ^{CS} with across different fluids observed in Fig. 4. Note that these values are significantly higher than those reported in [9] due to different partitioning criteria applied [12].

Fig. 5b shows that the ψ_S^k are larger than ϕ_S, which means that in this case the small particles bear larger kinetic pressure than their volume fraction allow. According to shear-induced segregation [9], particles which support a larger portion of P^k segregate towards the region of high shear – near the rough base. The relationship between the ψ_i^k and ϕ_i also shows a more noticeable change with the type of fluids. As the fluid becomes more viscous the curve diminishes. This implies that the increased viscosity dampens individual particle fluctuations which then results to a weaker tendency to segregate.

5 Conclusion

Through the analysis of segregation forcing terms derived from mixture theory and from stress partition arguments, we determine that fluid affects segregation in two major ways. Buoyant forces reduce contact stress gradients necessary in driving the upward percolation of large particles. However, buoyant effects cannot account for the weakening of segregation with viscosity since the decrease in particle contact interactions is complemented by the decrease in the bulk particle weight.

Increasing the viscosity dampens individual particle fluctuations, evident from the noticeable decrease of kinetic pressures. Physically, this may be interpreted that reduced particle random movement inhibits the generation of random voids which, when coupled with the reduced energetic motion, decreases the probability of small particles to fit into the available voids, leading to an overall reduction in the downward percolation velocity of small particles.

Acknowledgements

The authors acknowledge financial support from the National Natural Science Foundation of China (grant nos. 41941017, 11672318), Key Research Program of Frontier Sciences, Chinese Academy of Sciences (CAS) (grant no. QYZDB-SSW-DQC010), CAS 'Light of West China' Program and the CAS-TWAS President's Fellowship for International PhD students.

References

[1] L. Jing, C.Y. Kwok, Y.F. Leung, Phys. Rev. Lett., **118**, 118001 (2017)

[2] K. Van Der Vaart, P. Gajjar, G. Epely-Chauvin, N. Andreini, J.M.N.T. Gray, C. Ancey, Phys. Rev. Lett., **114**, 238001 (2015)

[3] J.M.N.T. Gray, Annu. Rev. Fluid Mech, **50**, 407 (2018)

[4] P.B. Umbanhowar, R.M. Lueptow, J.M. Ottino, Annu. Rev. Chem. Biomol. Eng., **10**, 5 (2019)

[5] J.M.N.T. Gray, V.A. Chugunov, J. Fluid Mech., **569**, 365 (2006)

[6] R.M. Iverson, Rev. Geophys., **35**, 245 (1997)

[7] T. Mulder and J. Alexander, Sedimentology, **48**, 269 (2001)

[8] A.R. Thornton, J.M.N.T. Gray, A.J. Hogg, J. Fluid Mech., **550**, 1 (2006)

[9] K.M. Hill, D.S. Tan, J. Fluid Mech., **756**, 54 (2014)

[10] T. Zhao, *Coupled DEM-CFD analyses of landslide-induced debris flows* (McGraw-Hill, Singapore, 2017)

[11] P.P. Brown, D.F. Lawler, J. Environ. Eng., **129**, 222 (2003)

[12] G.D. Zhou, K.F. Cui, L. Jing, T. Zhao, D.R. Song, and Y. Huang, J. Geophys. Res. Solid Earth, **125**, 1 (2020)